Phase noise characteristics of microwave signals generated by semiconductor laser dynamics

Jun-Ping Zhuang[1] **and Sze-Chun Chan**[1,2]

[1]*Department of Electronic Engineering, City University of Hong Kong, Hong Kong, China*
[2]*State Key Laboratory of Millimeter Waves, City University of Hong Kong, Hong Kong, China*
[*]*scchan@cityu.edu.hk*

Abstract: Phase noise of the period-one (P1) nonlinear dynamical oscillation in an optically injected semiconductor laser is numerically investigated. The P1 dynamics causes the laser output intensity to oscillate at a widely tunable frequency for photonic microwave generation, although the intrinsic spontaneous emission in the laser inevitably degrades the microwave signal and manifests as the oscillation phase noise. To characterize the phase noise, the P1 microwave linewidth is first numerically examined through the rate equations with a Langevin term. The P1 microwave linewidth is found to vary with the injection parameters. It is nearly minimized when the microwave power maximizes. Owing to the laser nonlinearities, the P1 microwave linewidth can even be smaller than the free-running optical linewidth. By adding an optical feedback to the laser, the P1 microwave linewidth is found to reduce as the feedback strength and feedback delay increase, in which an inverse-square dependency is followed asymptotically. By modification to a dual-loop feedback, noisy side peaks around the central P1 frequency are effectively suppressed through the Vernier effect. The dual-loop feedback maintains a low phase noise variance over a wide tuning range of the P1 frequency, while allowing long delay times for significant P1 microwave linewidth narrowing.

OCIS codes: (140.5960) Semiconductor lasers; (140.3520) Lasers, injection-locked; (350.4010) Microwaves; (190.3100) Instabilities and chaos.

References and links

1. T. B. Simpson, J. M. Liu, M. AlMulla, N. G. Usechak, and V. Kovanis, "Limit-cycle dynamics with reduced sensitivity to perturbations," Phys. Rev. Lett. **112**, 023901 (2014).
2. T. B. Simpson, J. M. Liu, M. AlMulla, N. G. Usechak, and V. Kovanis, "Linewidth sharpening via polarization-rotated feedback in optically injected semiconductor laser oscillators," IEEE J. Sel. Top. Quantum Electron. **19**, 1500807 (2013).
3. A. Quirce and A. Valle, "High-frequency microwave signal generation using multi-transverse mode VCSELs subject to two-frequency optical injection," Opt. Express **20**, 13390–13401 (2012).
4. H. Lin, D. W. Pierce, A. J. Basnet, A. Quirce, Y. Zhang, and A. Valle, "Two-frequency injection on a multimode vertical-cavity surface-emitting laser," Opt. Express **19**, 22437–22442 (2011).
5. M. Pochet, T. Locke, and N. G. Usechak, "Generation and modulation of a millimeter-wave subcarrier on an optical frequency generated via optical injection," IEEE Photon. J. **4**, 1881–1891 (2012).

#224479 - $15.00 USD Received 7 Oct 2014; revised 11 Jan 2015; accepted 15 Jan 2015; published 30 Jan 2015

6. M. Pochet, N. A. Naderi, V. Kovanis, and L. F. Lester, "Modeling the dynamic response of an optically-injected nanostructure diode laser," IEEE J. Quantum Electron. **47**, 827–833 (2011).
7. A. Hurtado, I. D. Henning, M. J. Adams, and L. F. Lester, "Generation of tunable millimeter-wave and THz signals with an optically injected quantum dot distributed feedback laser," IEEE Photon. J. **5**, 5900107 (2013).
8. Y. H. Liao and F. Y. Lin, "Dynamical characteristics and their applications of semiconductor lasers subject to both optical injection and optical feedback," Opt. Express **21**, 23568–23578 (2013).
9. Y. S. Juan and F. Y. Lin, "Photonic generation of broadly tunable microwave signals utilizing a dual-beam optically injected semiconductor laser," IEEE Photon. J. **3**, 644–650 (2011).
10. Y. H. Hung and S. K. Hwang, "Photonic microwave amplification for radio-over-fiber links using period-one nonlinear dynamics of semiconductor lasers," Opt. Lett. **38**, 3355–3358 (2013).
11. Y. H. Hung, C. H. Chu, and S. K. Hwang, "Optical double-sideband modulation to single-sideband modulation conversion using period-one nonlinear dynamics of semiconductor lasers for radio-over-fiber links," Opt. Lett. **38**, 1482–1484 (2013).
12. S. C. Chan, S. K. Hwang, and J. M. Liu, "Period-one oscillation for photonic microwave transmission using an optically injected semiconductor laser," Opt. Express **15**, 14921–14935 (2007).
13. S. C. Chan, "Analysis of an optically injected semiconductor laser for microwave generation," IEEE J. Quantum Electron. **46**, 421–428 (2010).
14. J. Capmany and D. Novak, "Microwave photonics combines two worlds," Nat. Photon. **1**, 319–330 (2007).
15. J. P. Yao, "Microwave photonics," J. Lightwave Technol. **27**, 314–335 (2009).
16. X. Q. Qi and J. M. Liu, "Photonic microwave applications of the dynamics of semiconductor lasers," IEEE J. Sel. Top. Quantum Electron. **17**, 1198–1211 (2011).
17. L. F. Lester, N. A. Naderi, F. Grillot, R. Raghunathan, and V. Kovanis, "Strong optical injection and the differential gain in a quantum dash laser," Opt. Express **22**, 7222–7228 (2014).
18. F. Grillot, C. Wang, N. A. Naderi, and J. Even, "Modulation properties of self-injected quantum-dot semiconductor diode lasers," IEEE J. Sel. Top. Quantum Electron. **19**, 1900812 (2013).
19. S. Wieczorek, W. W. Chow, L. Chrostowski, and C. J. Chang-Hasnain, "Improved semiconductor-laser dynamics from induced population pulsation," IEEE J. Quantum Electron. **42**, 552–562 (2006).
20. B. Bortnik, Y. C. Hung, H. Tazawa, B. J. Seo, J. Luo, A. K. Y. Jen, W. H. Steier, and H. R. Fetterman, "Electrooptic polymer ring resonator modulation up to 165 GHz," IEEE J. Sel. Top. Quantum Electron. **13**, 104–110 (2007).
21. R. J. Steed, L. Ponnampalam, M. J. Fice, C. C. Renaud, D. C. Rogers, D. G. Moodie, G. D. Maxwell, I. F. Lealman, M. J. Robertson, L. Pavlovic, L. Naglic, M. Vidmar, and A. J. Seeds, "Hybrid integrated optical phase-lock loops for photonic terahertz sources," IEEE J. Sel. Top. Quantum Electron. **17**, 210–217 (2011).
22. E. Sooudi, C. de Dios Fernandez, J. G. McInerney, G. Huyet, F. Lelarge, K. Merghem, R. Rosales, A. Martinez, A. Ramdane, and S. P. Hegarty, "A novel scheme for two-level stabilization of semiconductor mode-locked lasers using simultaneous optical injection and optical feedback," IEEE J. Sel. Top. Quantum Electron. **19**, 1101208 (2013).
23. M. J. Strain, M. Zanola, G. Mezosi, and M. Sorel, "Generation of picosecond pulses over a 40-nm wavelength range using an array of distributed Bragg grating mode-locked lasers," IEEE Photon. Technol. Lett. **25**, 368–370 (2013).
24. M. Haji, L. P. Hou, A. E. Kelly, J. Akbar, J. H. Marsh, J. M. Arnold, and C. N. Ironside, "High frequency optoelectronic oscillators based on the optical feedback of semiconductor mode-locked laser diodes," Opt. Express **20**, 3268–3274 (2012).
25. R. Rosales, K. Merghem, A. Martinez, A. Akrout, J. P. Tourrenc, A. Accard, F. Lelarge, and A. Ramdane, "InAs/InP quantum-dot passively mode-locked lasers for 1.55-μm applications," IEEE J. Sel. Top. Quantum Electron. **17**, 1292–1301 (2011).
26. C. Y. Lin, F. Grillot, Y. Li, R. Raghunathan, and L. F. Lester, "Microwave characterization and stabilization of timing jitter in a quantum-dot passively mode-locked laser via external optical feedback," IEEE J. Sel. Top. Quantum Electron. **17**, 1311–1317 (2011).
27. F. Tian, J. Chen, and G. F. Li, "Amplitude and phase noise of self-pulsations in laser diodes," Electron. Lett. **33**, 312–312 (1997).
28. X. Wang, G. F. Li, and C. S. Ih, "Microwave/millimeter-wave frequency subcarrier lightwave modulations based on self-sustained pulsation of laser diode," J. Lightwave Technol. **11**, 309–315 (1993).
29. J. B. Georges and K. Y. Lau, "Self-pulsating laser diodes as fast-tunable ($\leq$ 1 ns) FSK transmitters in subcarrier multiple-access networks," IEEE Photon. Technol. Lett. **5**, 242–245 (1993).
30. J. Renaudier, G. H. Duan, P. Landais, and P. Gallion, "Phase correlation and linewidth reduction of 40 GHz self-pulsation in distributed Bragg reflector semiconductor lasers," IEEE J. Quantum Electron. **43**, 147–156 (2007).
31. O. Carroll, Y. Tanguy, J. Houlihan, and G. Huyet, "Dynamics of self-pulsing semiconductor lasers with optical feedback," Opt. Commun. **239**, 429–436 (2004).
32. M. Al-Mumin, X. Wang, W. Mao, S. Pappert, and G. F. Li, "Optical generation and sideband injection locking of tunable 11-120 GHz microwave/millimetre signals," Electron. Lett. **36**, 1547–1548 (2000).
33. X. H. Wang and G. F. Li, "Subcarrier frequency enhancement of two-section Fabry-Perot laser diodes using external optical injection," Opt. Commun. **171**, 113–118 (1999).

#224479 - $15.00 USD Received 7 Oct 2014; revised 11 Jan 2015; accepted 15 Jan 2015; published 30 Jan 2015

34. G. F. Li, D. M Nair, and K. M. Magde, "Amplitude and phase noise of periodic orbits in a nonlinear optical system: theory and experiments," IEEE LEOS Annual Meeting Proc. **2**, 178–179 (1997).
35. B. Romeira, J. Javaloyes, J. M. L. Figueiredo, C. N. Ironside, H. I. Cantu, and A. E. Kelly, "Delayed feedback dynamics of Lienard-type resonant tunneling-photo-detector optoelectronic oscillators," IEEE J. Quantum Electron. **49**, 31–42 (2013).
36. J. Y. Kim, J. H. Jo, W. Y. Choi, and H. K. Sung, "Dual-loop dual-modulation optoelectronic oscillators with highly suppressed spurious tones," IEEE Photon. Technol. Lett. **24**, 706–708 (2012).
37. S. L. Pan and J. P. Yao, "Wideband and frequency-tunable microwave generation using an optoelectronic oscillator incorporating a Fabry-Perot laser diode with external optical injection," Opt. Lett. **35**, 1911–1913 (2010).
38. X. S. Yao and L. Maleki, "Multiloop optoelectronic oscillator," IEEE J. Quantum Electron. **36**, 79–84 (2000).
39. X. S. Yao and L. Maleki, "Optoelectronic microwave oscillator," J. Opt. Soc. Am. B **13**, 1725–1735 (1996).
40. F. Li and A. S. Helmy, "Gigahertz to terahertz tunable all-optical single-side-band microwave generation via semiconductor optical amplifier gain engineering," Opt. Lett. **38**, 4542–4545 (2013).
41. Y. N. Tan, L. Jin, L. Cheng, Z. Quan, M. Li, and B. O. Guan, "Multi-octave tunable RF signal generation based on a dual-polarization fiber grating laser," Opt. Express **20**, 6961–6967 (2012).
42. G. Carpintero, E. Rouvalis, K. Lawniczuk, M. Fice, C. C. Renaud, X. J. M. Leijtens, E. A. J. M. Bente, M. Chitoui, F. V. Dijk, and A. J. Seeds, "95 GHz millimeter wave signal generation using an arrayed waveguide grating dual wavelength semiconductor laser," Opt. Lett. **37**, 3657–3659 (2012).
43. M. Zanola, M. J. Strain, G. Giuliani, and M. Sorel, "Monolithically integrated DFB lasers for tunable and narrow linewidth millimeter-wave generation," IEEE J. Sel. Topics Quantum Electron. **19**, 1500406 (2013).
44. S. Donati and S. K. Hwang, "Chaos and high-level dynamics in coupled lasers and their applications," Prog. Quantum Electron. **36**, 293–341 (2012).
45. J. P. Zhuang and S. C. Chan, "Tunable photonic microwave generation using optically injected semiconductor laser dynamics with optical feedback stabilization," Opt. Lett. **38**, 344–346 (2013).
46. C. Cui and S. C. Chan, "Performance analysis on using period-one oscillation of optically injected semiconductor lasers for radio-over-fiber uplinks," IEEE J. Quantum Electron. **48**, 490–499 (2012).
47. C. Cui, X. Fu, and S. C. Chan, "Double-locked semiconductor laser for radio-over-fiber uplink transmission," Opt. Lett. **34**, 3821–3823 (2009).
48. J. B. Altes, I. Gatare, K. Panajotov, H. Thienpont, and M. Sciamanna, "Mapping of the dynamics induced by orthogonal optical injection in vertical-cavity surface-emitting lasers," IEEE J. Quantum Electron. **42**, 198–207 (2006).
49. M. S. Torre, C. Masoller, and K. A. Shore, "Numerical study of optical injection dynamics of vertical-cavity surface-emitting lasers," IEEE J. Quantum Electron. **40**, 25–30 (2004).
50. X. Q. Qi and J. M. Liu, "Dynamics scenarios of dual-beam optically injected semiconductor lasers," IEEE J. Quantum Electron. **47**, 762–769 (2011).
51. M. Zhang, T. Liu, A. Wang, J. Zhang, and Y. Wang, "All-optical clock frequency divider using Fabry-Perot laser diode based on the dynamical period-one oscillation," Opt. Commun. **284**, 1289–1294 (2011).
52. S. C. Chan and J. M. Liu, "Microwave frequency division and multiplication using an optically injected semiconductor laser," IEEE J. Quantum Electron. **41**, 1142–1147 (2005).
53. S. C. Chan, S. K. Hwang, and J. M. Liu, "Radio-over-fiber AM-to-FM upconversion using an optically injected semiconductor laser," Opt. Lett. **31**, 2254–2256 (2006).
54. C. H. Cheng, C. W. Lee, T. W. Lin, and F. Y. Lin, "Dual-frequency laser Doppler velocimeter for speckle noise reduction and coherence enhancement," Opt. Express **20**, 20255–20265 (2012).
55. T. B. Simpson and F. Doft, "Double-locked laser diode for microwave photonics applications," IEEE Photon. Technol. Lett. **11**, 1476–1478 (1999).
56. T. B. Simpson, "Phase-locked microwave-frequency modulations in optically-injected laser diodes," Opt. Commun. **170**, 93–98 (1999).
57. S. C. Chan and J. M. Liu, "Tunable narrow-linewidth photonic microwave generation using semiconductor laser dynamics," IEEE J. Sel. Top. Quantum Electron. **10**, 1025–1032 (2004).
58. K. H. Lo, S. K. Hwang, and S. Donati, "Optical feedback stabilization of photonic microwave generation using period-one nonlinear dynamics of semiconductor lasers," Opt. Express **22**, 18648–18661 (2014).
59. J. M. Liu, H. F. Chen, X. J. Meng, and T. B. Simpson, "Modulation bandwidth, noise, and stability of a semiconductor laser subject to strong injection locking," IEEE Photon. Technol. Lett. **9**, 1325–1327 (1997).
60. T. Erneux and P. Glorieux, *Laser Dynamics* (Cambridge Univ. Press, 2010).
61. S. S. Li, Q. Liu, and S. C. Chan, "Distributed feedbacks for time-delay signature suppression of chaos generated from a semiconductor laser," IEEE Photon. J. **4**, 1930–1935 (2012).
62. T. B. Simpson, J. M. Liu, K. F. Huang, and K. Tai, "Nonlinear dynamics induced by external optical injection in semiconductor lasers," Quantum Semiclass. Opt. **9**, 765–784 (1997).
63. C. Henry, "Phase noise in semiconductor lasers," J. Lightwave Technol. **4**, 298–311 (1986).
64. N. Zhang, X. Cai, and S. Yu, "Optical generation of tunable and narrow linewidth radio frequency signal based on mutual locking between integrated semiconductor lasers," Photon. Res. **2**, B11–B17 (2014).
65. P. M. Varangis, A. Gavrielides, V. Kovanis, and L. F. Lester, "Linewidth broadening across a dynamical instabil-

#224479 - $15.00 USD Received 7 Oct 2014; revised 11 Jan 2015; accepted 15 Jan 2015; published 30 Jan 2015

ity," Phys. Lett. A **250**, 117–122 (1998).
66. J. Ohtsubo, *Semiconductor Lasers: Stability, Instability and Chaos* (Springer, 2008).
67. K. Petermann, "External optical feedback phenomena in semiconductor lasers," IEEE J. Sel. Top. Quantum Electron. **1**, 480–489 (1995).
68. F. Kefelian, S. O'Donoghue, M. T. Todaro, J. G. McInerney, and G. Huyet, "RF linewidth in monolithic passively mode-locked semiconductor laser," IEEE Photon. Technol. Lett. **20**, 1405–1407 (2008).
69. O. Pottiez, O. Deparis, R. Kiyan, M. Haelterman, P. Emplit, P. Megret, and M. Blondel, "Supermode noise of harmonically mode-locked erbium fiber lasers with composite cavity," IEEE J. Quantum Electron. **38**, 252–259 (2002).

1. Introduction

Nonlinear dynamical period-one (P1) oscillations in optically injected semiconductor lasers have been actively investigated for photonic microwave generation [1–13]. Photonic microwave generation enables the transmission of microwave signals over optical fibers with no electromagnetic interference and low propagation loss [14–16]. Approaches adopting high-frequency electronic sources for photonic microwave generation include direct modulation on injection-locked lasers [17–19], external modulation using electrooptic materials [20], and side-band locking along with phase-lock loops on modulated light sources [21], which can yield very low phase noise depending on the electronic sources. However, there are also several approaches requiring no high-frequency electronic sources for photonic microwave generation. For example, mode-locked laser diodes (MLLDs) are excellent for monolithically generating photonic microwave tones at the pulse repetition rates. The frequency tunability is limited by the fixed cavity lengths, though some injection and feedback schemes were recently employed to improve the frequency stability and time-bandwidth products in MLLDs [22–26]. Two-section lasers with proper cavity designs had led to pioneering works on self-pulsation phenomena [27–29], which can be observed even without involving any external perturbations. Interesting analysis and modeling of the phase noise associated with the self-pulsations have been reported [30–34]. The optoelectronic oscillators (OEOs) also require no electronic sources to generate microwave signals. Employing long fiber-based feedback loops yield excellent stabilities, though the loops still incorporate high-frequency electronic filters and detectors. Replacing these electronic devices with photonic devices can further improve the tunability and other performances of OEOs [35–39]. Dual-wavelength operation was implemented in fiber lasers to generate microwave frequencies by proper seeding from independent lasers or by different gratings with mechanical or thermal tuning [40, 41]. It was also monolithically implemented in semiconductor lasers with arrayed waveguide gratings to yield discrete tunability [42]. A monolithic approach with three mutually injected lasers was also investigated recently for microwave generation tunable up to 40 GHz, where a clear microwave linewidth reduction to 2.5 MHz was attained by mutual locking through frequency mixing [43].

The nonlinear dynamical P1 oscillation has emerged as an interesting alternative to photonic microwave generation [1, 16]. The P1 oscillation is among a variety of nonlinear dynamics such as period-doubled, quasi-periodic, and chaotic oscillations for lasers under continuous-wave (CW) injections. The P1 oscillation is obtained when a stably locked laser experiences a Hopf bifurcation, which generates a modulation of the laser emission intensity at a microwave frequency [1, 13, 44]. The P1 oscillation has been investigated in conventional single-mode distributed feedback (DFB) lasers [1, 2, 45–47], quantum-dash or quantum-dot lasers [5–7], as well as vertical-cavity surface-emitting lasers (VCSELs) [3, 4, 48, 49]. Dual-wavelength injection and multi-transverse mode injection have also been reported for generating photonic microwave signals [3, 9, 50].

For photonic microwave generation, the nonlinear dynamical P1 oscillation offers the following advantages [16]. The P1 frequency is widely tunable beyond the original relaxation

#224479 - $15.00 USD Received 7 Oct 2014; revised 11 Jan 2015; accepted 15 Jan 2015; published 30 Jan 2015

resonance frequency, reaching even the terahertz band [6, 7]. The P1 oscillation generates photonic microwave signals all-optically without using any electronic microwave sources [2, 16]. Single sideband (SSB) optical spectra are attainable by adjusting the injection parameters with the benefit of minimizing the microwave power penalty during transmission through dispersive fibers [10–12, 46]. Intensity modulation depth of nearly 100% can be attained for generating maximal microwave power at a constant optical average power [5, 10]. Data modulation on the microwave signal can be realized by modulating the laser bias current electrically or the injection optically [5, 47]. These advantages were utilized in a number of applications such as radio-over-fiber downlink transmission [5], uplink transmission [46, 47], clock frequency division [51, 52], modulation format conversion [11, 53], photonic microwave amplification [10], and Doppler velocimeter with long detection ranges [54].

In spite of these advantages, the P1 oscillation dynamics inherently contains phase noise due to fluctuations in the lasers. The phase noise causes adverse effects such as reductions of the signal-to-noise ratios in communication links [5], degradations of the noise performance in photonic microwave amplification [10], and limitations of the maximal detection range in Doppler velocimeters [54]. For instance, the velocity resolution degrades within a few meters using a P1 oscillation with a 13.9-MHz microwave linewidth [54]. As a result, some techniques were developed for reducing the phase noise. Experiments have demonstrated double-locking using a microwave source [55, 56], optoelectronic feedback employing an electronic feedback loop [57], and polarization-rotated feedback added with the optoelectronic feedback [2], where a reduced linewidth of about 3 kHz was obtained for P1 oscillation at 6 GHz. To avoid the frequency limitations of high-speed electronics, a dual-loop optical feedback was demonstrated as an all-optical approach with the P1 oscillation frequency increased to over 45 GHz while maintaining a narrow linewidth below 50 kHz [45]. Such a dual-loop feedback on P1 oscillation required no high-speed electronics, demonstrated wide frequency tunability, and significantly reduced both the microwave linewidth as well as the phase variance [45]. However, there were few reports investigating the P1 oscillation noise numerically. Interesting operating points with the P1 oscillation frequency being insensitive to the injection detuning frequency were identified from recent simulations [1]. Data transmission performances were reported by modeling the operational noise of the pump or injection [5]. Nonetheless, the influences of the intrinsic spontaneous emission noise on the P1 oscillation remain to be systematically investigated.

In this paper, the phase noise of the P1 oscillation due to the spontaneous emissions in the injected laser is investigated numerically. As a fundamental noise source intrinsic to the laser, spontaneous emission is modeled by a Langevin fluctuation force in the rate-equation model, causing phase noise in the P1 oscillation, which broadens the P1 microwave linewidth. To begin with, only optical injection is applied to invoke the P1 oscillation. The P1 microwave linewidth is found to vary with the injection parameters. It is minimized when the amplitude of the intensity oscillation maximizes at any given P1 frequency. Interestingly, the P1 microwave linewidth can be even smaller than the free-running optical linewidth, which is impossible without nonlinear interactions in the laser. Moreover, by adding a single-loop optical feedback to the laser, the P1 microwave linewidth is observed to clearly reduce. The linewidth is found as inversely proportional to the square of the feedback strength. It is also found as inversely proportional to the square of the feedback delay time. However, noisy side peaks in the power spectrum are enhanced as the delay lengthens, which prompts the use of a dual-loop optical feedback. The dual-loop optical feedback is found to significantly suppress the side peaks though the Vernier effect when the delay times are incommensurate. So the dual-loop feedback enables microwave linewidth narrowing by adopting long feedback delay times, while keeping a low phase variance regardless of the P1 oscillation frequency. With a free-running optical linewidth of 100 MHz, the laser in P1 oscillation at 24 GHz gives a microwave linewidth of 22 MHz, which is then

#224479 - $15.00 USD Received 7 Oct 2014; revised 11 Jan 2015; accepted 15 Jan 2015; published 30 Jan 2015

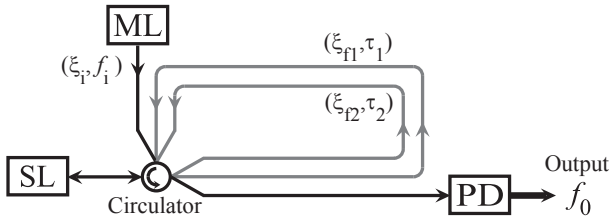

Fig. 1. Schematic of an optically injected laser with optical feedback for photonic microwave generation. The black lines indicate the path of optical injection from ML to SL for invoking the P1 oscillation. The gray lines indicate two optional optical feedback paths for reducing the phase noise of the P1 oscillation. SL: slave laser. ML: master laser. PD: photodetector.

reduced to 4 kHz and 200 Hz by proper single-loop and dual-loop feedbacks, respectively.

Overall, the numerical results are qualitatively consistent with the previously reported experiments on dual-loop optical feedback [45]. The results also complement the latest report on the laser dynamics with a short single-loop feedback [58], which involves severe mode competition that can degrade the frequency purity of the P1 oscillation. It is also worth mentioning some early investigations of oscillatory nonlinear dynamics with noise modeling in self-pulsating two-section lasers [34]. Following this introduction, the simulation model is presented in Section 2. The P1 oscillation generated by the optical injection without any feedback is investigated in Section 3. The effects of single-loop and dual-loop feedback are studied in Sections 4 and 5, respectively. A discussion in Section 6 is then followed by a conclusion in Section 7.

2. Simulation model

Figure 1 shows the schematic for photonic microwave generation using P1 oscillation induced by optical injection with phase noise reduction by optical feedback. The schematic resembles that previously adopted in an experimental work [45]. CW light from a master laser unidirectionally injects into a slave laser through an optical circulator. The slave laser is a single-mode semiconductor laser biased above its threshold. The injection is specified by parameters (ξ_i, f_i). The injection strength ξ_i is a normalized quantity proportional to the injection field, while the injection detuning frequency f_i is the difference of the injection optical frequency from the free-running optical frequency of the slave laser [13, 59]. The P1 oscillation is invoked in the slave laser when the detuning frequency is above the Hopf bifurcation line in the injection parameter space [60]. The emission of the slave laser carries a modulation at a microwave frequency f_0 due to the P1 oscillation [16]. This generates optical frequency components separated by f_0 from the injected optical frequency in the optical spectrum. Through the circulator, the slave laser emission is converted by a photodetector into a microwave output signal at f_0 [12].

Even with a stable CW injection from the master laser, the slave laser is inherently influenced by its spontaneous emission noise, which gives rise to phase noise of the P1 oscillation. To reduce the phase noise, optical feedback loops are added to the slave laser, as the gray lines in Fig. 1 show. Light from the slave laser passes the circulator into the loops and is then fed back optically to the slave laser. One loop is sufficient to narrow the microwave linewidth of the central peak, though two loops are adopted to suppress the side peaks in the power spectrum [45]. The two loops are specified by the optical feedback parameters (ξ_{f1}, τ_1) and (ξ_{f2}, τ_2), respectively. The feedback strengths ξ_{f1} and ξ_{f2} are normalized quantities proportional to the feedback fields through the respective loops back into the slave laser, where the total feedback strength $\xi_f = \xi_{f1} + \xi_{f2}$ is in practice limited by the optical coupling efficiency from the slave

#224479 - $15.00 USD Received 7 Oct 2014; revised 11 Jan 2015; accepted 15 Jan 2015; published 30 Jan 2015

laser into the circulator [44]. The feedback delay times τ_1 and τ_2 are the group delays of the optical signal emitting from and returning to the slave laser through the respective loops [61]. The slave laser, injection, and feedbacks are assumed to have aligned polarizations. The phase differences are ignored as they do not show strong influences on the oscillation noise in the following simulation results.

The dynamics of the slave laser is described by the intracavity optical field amplitude $A(t)$ and the charge carrier density $N(t)$. The field amplitude is a complex phasor quantity with respect to the free-running optical frequency of the slave laser. For convenience, the field amplitude is normalized to $a = A/|A_0|$ and the charge carrier density is normalized to $\tilde{n} = (N - N_0)/N_0$, where A_0 and N_0 are respectively the free-running values of A and N. The slave laser is modeled by the following rate equations [13, 59]:

$$\begin{aligned} \frac{da}{dt} &= \frac{1-ib}{2}\left[\frac{\gamma_c\gamma_n}{\gamma_s\tilde{J}}\tilde{n} - \gamma_p(|a|^2-1)\right]a + \xi_i\gamma_c e^{-i2\pi f_i t} + f \\ &\quad + \xi_{f1}\gamma_c a(t-\tau_1) + \xi_{f2}\gamma_c a(t-\tau_2), \qquad (1) \\ \frac{d\tilde{n}}{dt} &= -\left(\gamma_s + \gamma_n|a|^2\right)\tilde{n} - \gamma_s\tilde{J}\left(1 - \frac{\gamma_p}{\gamma_c}|a|^2\right)(|a|^2-1), \qquad (2) \end{aligned}$$

where γ_c is the cavity decay rate, γ_s is the spontaneous carrier relaxation rate, γ_n is the differential carrier relaxation rate, γ_p is the nonlinear carrier relaxation rate, b is the linewidth enhancement factor, and $\tilde{J}$ is the normalized bias current above threshold. The term with ξ_i represents the optical injection [6, 12, 44]. The terms with ξ_{f1} and ξ_{f2} represent the optical feedbacks from the two loops [61].

A Langevin fluctuating force f is included in Eq. (1) to account for the spontaneous emission noise of the slave laser [59, 62]. Its real and imaginary parts are mutually independent. The Langevin force at different times are also independent, where ergodicity is observed with the following averages:

$$\begin{aligned} < f(t)f^*(t') > &= \frac{4\pi\Delta\nu}{1+b^2}\delta(t-t'), \qquad (3) \\ < f(t)f(t') > &= 0, \qquad (4) \\ < f(t) > &= 0. \qquad (5) \end{aligned}$$

Here, $\Delta\nu$ is the full width at half-maximum (FWHM) optical linewidth when the slave laser is free-running [63]. Unlike other environmental fluctuations such as temperature and detuning variations, the spontaneous emission noise represented by f is intrinsic to the slave laser and cannot be avoided. In the simulations, the FWHM optical linewidth of the free-running slave laser is taken as $\Delta\nu = 100$ MHz [3]. The parameters from a typical semiconductor laser are adopted [12]: $\gamma_c = 5.36\times10^{11}$ s^{-1}, $\gamma_s = 5.96\times10^{9}$ s^{-1}, $\gamma_n = 7.53\times10^{9}$ s^{-1}, $\gamma_p = 1.91\times10^{10}$ s^{-1}, $b = 3.2$, and $\tilde{J} = 1.222$. They correspond to a relaxation resonance frequency of $f_r = 10.25$ GHz. Second-order Runge-Kutta integration is conducted on Eqs. (1)–(2). The optical spectrum and power spectrum of the slave laser emission are obtained by applying the Fourier transform on $a(t)$ and $|a(t)|^2$, respectively. The optical spectrum directly corresponds to the slave laser emission light, whereas the power spectrum corresponds to the microwave output of the photodetector in Fig. 1. The numerical integration has a time step of 0.93 ps. It is carried over a time span of effectively up to 1.05 ms, which is orders of magnitude longer than those reported in most related works [1, 12, 16]. The long time span enables high spectral resolution for examining the narrow microwave linewidths.

#224479 - $15.00 USD Received 7 Oct 2014; revised 11 Jan 2015; accepted 15 Jan 2015; published 30 Jan 2015

3. Optical injection-induced P1

The P1 oscillation is invoked in the slave laser by optical injection alone without applying any optical feedback. The optical injection parameters (ξ_i, f_i) determine the P1 oscillation frequency f_0. The optical feedback strengths ξ_{f1} and ξ_{f2} are set to zero. The variation of the P1 microwave linewidth at different oscillation frequencies is examined in this section. Figures 2(a)–2(d) show the optical spectra and the power spectra of the slave laser emission under P1 oscillations of different frequencies f_0. The resolution bandwidths of the optical and power spectra are 8 MHz and 0.06 MHz, respectively. The optical spectra are offset to the optical frequency of the free-running slave laser, while the power spectra are centered at the respective P1 oscillation frequencies f_0. For each value of f_0 in Fig. 2, the injection parameters are chosen to maximize the microwave power, which corresponds to maximizing the intensity modulation depth in the time-domain intensity waveforms. The intensity modulation depth is found to exceed 94% under the injection parameters in Fig. 2. Throughout this work, the microwave power is estimated by integrating the power spectrum over ± 1 GHz around f_0, where the microwave harmonics at multiples of f_0 are at least 20 dB weaker than the fundamental and are hence ignored.

3.1. Microwave linewidth Δf_0 versus frequency f_0

In Fig. 2(a) with (ξ_i, f_i) = (0.03, 4.0 GHz), the slave laser exhibits P1 oscillation at f_0 = 10.2 GHz. From the optical spectrum in Fig. 2(a-i), the optical injection with detuning frequency f_i is regenerated in the slave laser as the red arrow indicates. The P1 dynamics gives rise to a number of optical sidebands separated by multiples of the P1 frequency f_0 from the regenerative component. These optical sidebands generate a beat signal at f_0 in the power spectrum, as Fig. 2(a-ii) shows. However, the spontaneous emission noise represented by the Langevin fluctuating force broadens the optical linewidths of the optical sidebands. It also broadens the microwave linewidth at f_0 in the power spectrum, which has a FWHW microwave linewidth of Δf_0 = 55 MHz based on a Lorentzian fit.

In Fig. 2(b) with (ξ_i, f_i) = (0.12, 7.0 GHz), the P1 frequency f_0 increases to 18 GHz. The optical spectrum in Fig. 2(b-i) again contains the regenerative component at f_i and the optical sidebands separated by multiples of f_0. The strongest components of the optical spectrum are the regenerative component at f_i and its first lower sideband at $f_i - f_0$. The two components are of equal amplitude and so attain the maximal intensity modulation depth of 100% [12]. The power spectrum in Fig. 2(b-ii) shows the beat signal at f_0, which has a narrower microwave linewidth Δf_0 = 14 MHz. This is actually the narrowest microwave linewidth of P1 oscillation if no feedback is applied. Interestingly, the P1 microwave linewidth Δf_0 is even narrower than the free-running optical linewidth $\Delta\nu$ of the laser. The narrow linewidth is allowed by the nonlinear frequency mixing among a number of optical frequency components in the P1 optical spectrum of Fig. 2(b-i). The P1 oscillation is not exactly the same as heterodyning the injection light with a free-running slave laser [12,13]. Similar narrowing of microwave linewidth through nonlinear frequency mixing was also reported in mutually coupled three-laser systems with DFB lasers as well as semiconductor ring lasers (SRLs) [43, 64].

In Fig. 2(c) with (ξ_i, f_i) = (0.17, 14.2 GHz), the P1 frequency f_0 increases to 24 GHz. The associated microwave linewidth slightly degrades to Δf_0 = 22 MHz. In Fig. 2(d) with (ξ_i, f_i) = (0.48, 55.5 GHz), the P1 frequency f_0 continually increases to 60 GHz, which is much greater than the relaxation resonance frequency f_r of the laser. From the optical spectrum in Fig. 2(d-i), the components at f_i and $f_i - f_0$ are now much more dominating, in which they are at least 30 dB stronger than the rest of the sidebands. According to a two-wavelength approximation, the component at f_i is simply the regeneration of the emission, while the component at $f_i - f_0$ is the emission of the slave laser near its cavity resonance [13]. The slave laser is different from

#224479 - $15.00 USD Received 7 Oct 2014; revised 11 Jan 2015; accepted 15 Jan 2015; published 30 Jan 2015

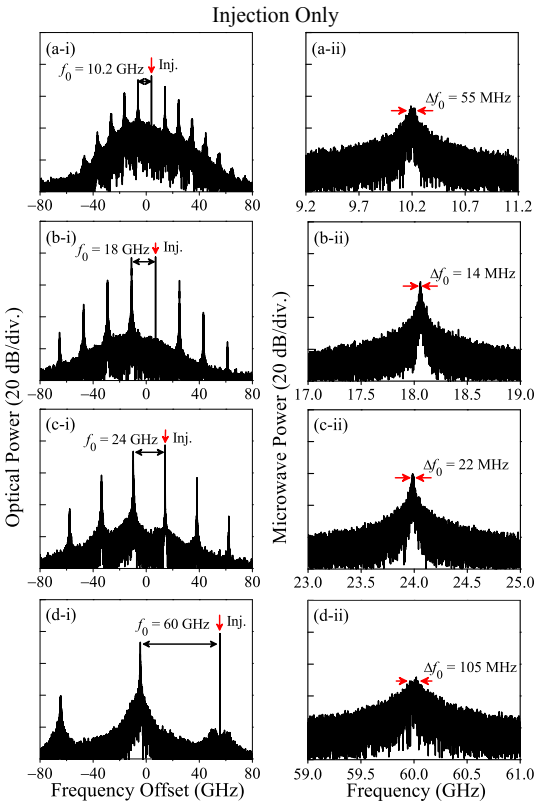

Fig. 2. (i) Optical spectra and (ii) power spectra of the slave laser emission subject to optical injection alone without any feedback. The laser is driven into P1 oscillation at frequency f_0 = (a) 10.2 GHz, (b) 18 GHz, (c) 24 GHz, and (d) 60 GHz by using injection parameters (ξ_i, f_i) = (0.03, 4.0 GHz), (0.12, 7.0 GHz), (0.17, 14.2 GHz), and (0.48, 55.5 GHz), respectively. The injection parameters are chosen to maximize the microwave power for each f_0. The microwave linewidth Δf_0 is labeled in each power spectrum.

being free-running because its cavity resonance is red-shifted by the injection. Strong injection can suppress the emission power at $f_i - f_0$ and thereby can increase the optical linewidth at $f_i - f_0$ beyond $\Delta\nu$ [63]. Through beating with the regenerative component, the component at $f_i - f_0$ produces the power spectrum in Fig. 2(d-ii). The microwave linewidth is increased to Δf_0 = 105 MHz, which is now larger than $\Delta\nu$. For maximal microwave power, further increasing f_0 requires increasing f_i. It is associated with reducing the emission power at $f_i - f_0$ with further degradation of Δf_0. In short, Fig. 2 illustrates the wide tunability of the P1 frequency f_0 beyond the relaxation resonance frequency f_r, though the associated microwave linewidth Δf_0 varies with the injection parameters.

3.2. *Microwave linewidth Δf_0 versus injection parameters (ξ_i, f_i)*

To systematically investigate the behavior of the P1 microwave linewidth Δf_0, Fig. 3 shows its contour map in the injection parameter space (ξ_i, f_i). The large blue region above the Hopf bifurcation line is a region of P1 oscillation. The blue contour map indicates the microwave linewidth Δf_0 of the P1 oscillation. At (ξ_i, f_i) = (0.12, 7.0 GHz), the yellow point in Fig. 3 gives the minimal linewidth of Δf_0 = 14 MHz. Such a minimal-linewidth point is attained at f_0

#224479 - $15.00 USD Received 7 Oct 2014; revised 11 Jan 2015; accepted 15 Jan 2015; published 30 Jan 2015

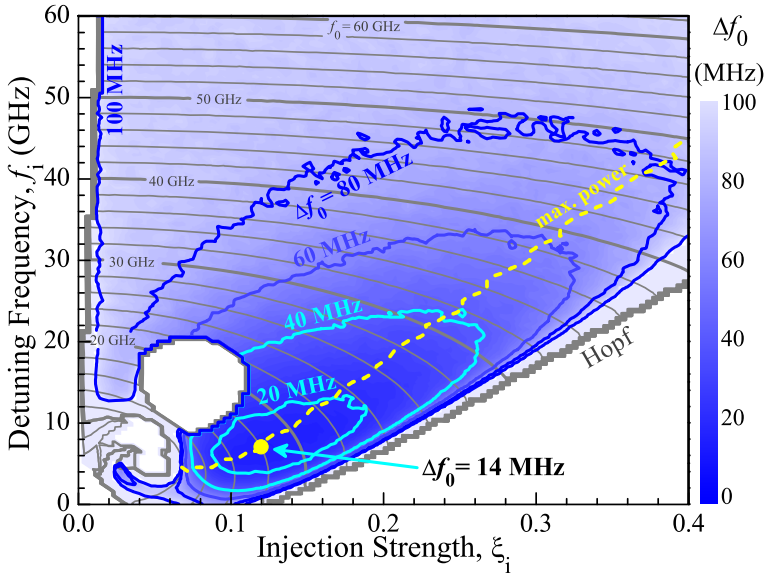

Fig. 3. Microwave linewidth Δf_0 as a contour map of the injection parameters (ξ_i, f_i). The blue contour lines are for the microwave linewidth Δf_0. The gray contour lines are for the P1 oscillation frequency f_0. The dashed line indicates the positions for maximal microwave power at any given f_0. The yellow dot is the minimal-linewidth point at (ξ_i, f_i) = (0.12, 7.0 GHz) with Δf_0 = 14 MHz.

= 18 GHz, as Fig. 2(b) shows. Then, when ξ_i goes to zero or when f_i increases much beyond f_r, Δf_0 increases up to around $\Delta\nu$ in Fig. 3. This is because the low-strength or largely detuned injection does not cause much nonlinear frequency mixing in the slave laser, so that the P1 oscillation reduces to a simple heterodyne process between the regenerated injection and the nearly free-running slave laser. However, when the Hopf bifurcation line in Fig. 3 is crossed, the slave laser becomes stably locked by the injection. The P1 oscillation becomes damped such that its linewidth quickly increases near the Hopf bifurcation line. Moreover, the slave laser also experiences period-doubling into other oscillatory states in the small white regions with (ξ_i, f_i) at around (0.08, 15 GHz) and (0.04, 8 GHz). These regions do not give P1 oscillation and need to be avoided in photonic microwave generation [12], where linewidth broadening at period-doubling bifurcations has been reported [65].

Within the region of P1 oscillation in blue, Fig. 3 also shows the gray contour lines of the P1 oscillation frequency f_0, which is widely and continuously tunable beyond the relaxation resonance frequency f_r as the injection parameters vary. Adjusting (ξ_i, f_i) along any of these contour lines keeps f_0 constant, while the associated microwave power varies. The dashed line in Fig. 3 indicates the positions of maximal microwave power at any given f_0. Comparing the dashed line with the map of Δf_0 reveals that, for any fixed f_0, the microwave linewidth is nearly minimized as the microwave power maximizes. For example, the minimal-linewidth point with Δf_0 = 14 MHz lies directly on the dashed line in Fig. 3 for f_0 = 18 GHz. Further increasing f_0 along the dashed line is associated with increasing Δf_0.

Interestingly, there are recent works focusing on points with the contour lines of f_0 being tangentially vertical, which ensure insensitivity of f_0 to variations of f_i [1, 2]. Such a detuning-insensitive point for f_0 = 18 GHz is at (ξ_i, f_i) = (0.125, 3.5 GHz) according to Fig. 3. However, the detuning-insensitive point is not the same as the minimal-linewidth point. This causes

#224479 - $15.00 USD Received 7 Oct 2014; revised 11 Jan 2015; accepted 15 Jan 2015; published 30 Jan 2015

no contradiction because the intrinsic spontaneous emission noise, rather than the detuning variation, is considered as the fundamental source of fluctuation here in Fig. 3. As for experimental investigations, the temperature fluctuations have not been totally eliminated thus far, so both detuning variations and spontaneous emissions contribute to the linewidth. The linewidth, nonetheless, was experimentally confirmed to vary with the injection parameters [2, 45].

Summarizing this section on optical injection, the P1 oscillation can have a microwave linewidth Δf_0 being smaller than the free-running optical linewidth $\Delta\nu$. Given a P1 microwave frequency f_0, its linewidth Δf_0 is nearly minimized when the microwave power maximizes. The P1 frequency f_0 can also be tuned much beyond f_r, but it is associated with increasing Δf_0. In order to reduce the microwave linewidth and phase noise, optical feedbacks on the P1 oscillation are considered in the following sections.

4. P1 with single-loop feedback

Linewidth reduction through single-loop optical feedback is considered in this section on the optically injected laser in P1 oscillation. Similar to a solitary laser without injection [66,67], the feedback loop stores the phase information, sets up external cavity modes, and causes reduction of the linewidth for the central peak along with residual side peaks separated by the reciprocal of the feedback delay time. In this section, the optical injection parameters are fixed at (ξ_i, f_i) = (0.17, 14.2 GHz). The laser enters P1 oscillation at f_0 = 24 GHz as in Fig. 2(c) prior to applying any feedback. To avoid losing generality, the injection parameters are chosen not to correspond to the minimum-linewidth point in Fig. 3 as the feedback is found to reduce the microwave linewidth regardless of the P1 frequency. Only one loop in Fig. 1 is turned on with feedback parameters (ξ_{f1}, τ_1) denoted simply as (ξ_f, τ), whilst the other loop remains off by keeping ξ_{f2} at zero. Figures 4(a)–4(d) show the optical and power spectra of the laser emission at different feedback strengths. The feedback delay time is fixed at $\tau = 2.4$ ns. The optical spectra are again offset to the free-running frequency of the laser. The power spectra are centered at 24 GHz. The resolution bandwidth of the optical spectra remains at 8 MHz, but that of the power spectra is decreased to 1 kHz for examining the narrow central peaks. The high-resolution spectra are made possible by the significantly increased effective simulation time-span compared to most earlier works [1, 12, 16].

In Fig. 4(a) with ξ_f = 0.010, the slave laser continues exhibiting P1 oscillation at f_0 = 24 GHz. The optical spectrum in Fig. 4(a-i) with feedback is essentially the same as that in Fig. 2(c-i) without feedback. The regenerative component indicated by the red arrow and the optical sidebands separated by multiples of f_0 are again identified. However, comparing with Fig. 2(c-ii), the power spectrum in Fig. 4(a-ii) shows a significant narrowing of the central peak at f_0. From the original Δf_0 = 22 MHz, the feedback significantly reduces the FWHM microwave linewidth down to $\Delta f_0'$ = 93 kHz. Although the feedback also invokes some side peaks equally separated from the central peak by multiples of $1/\tau$, these side peaks are much weaker than the central peak and so do not contribute to the FWHM linewidth. In Fig. 4(b), by increasing the feedback strength to ξ_f = 0.026, the microwave linewidth is further reduced. The power spectrum of Fig. 4(b-ii) shows the microwave linewidth narrowing to $\Delta f_0'$ = 9 kHz for the central peak, where the magnitudes of the side peaks are suppressed as well. The optical spectrum in Fig. 4(b-i) contains the same frequency components as before. Though the optical background noise is slightly enhanced in between the frequency components, it remains much weaker than the two strongest frequency components at f_i and $f_i - f_0$ by over 30 dB.

In Fig. 4(c), the feedback strength increases to ξ_f = 0.034. The power spectrum of Fig. 4(c-ii) shows that the microwave linewidth of the central peak further reduces to $\Delta f_0'$ = 4 kHz, which is over three orders of magnitude below Δf_0 prior to applying any feedback. From the optical spectrum in Fig. 4(c-i) the regenerative component at f_i and the sideband at $f_i - f_0$ are still

#224479 - $15.00 USD Received 7 Oct 2014; revised 11 Jan 2015; accepted 15 Jan 2015; published 30 Jan 2015

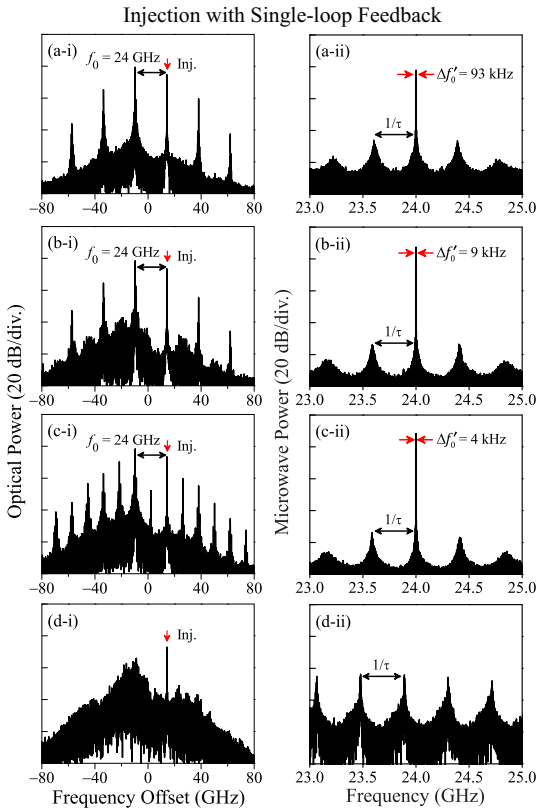

Fig. 4. (i) Optical spectra and (ii) power spectra of the slave laser emission subject to optical injection with single-loop feedback. The feedback strength ξ_f = (a) 0.010, (b) 0.026, (c) 0.034, and (d) 0.060. The feedback delay time is fixed at $\tau = 2.4$ ns. The injection parameters are fixed at (ξ_i, f_i) = (0.17, 14.2 GHz). The reduced microwave linewidth $\Delta f_0'$ is labeled for each central peak at f_0.

the two strongest components, yet subharmonic components emerge in between the original components because of proximity to a period-doubling bifurcation [52]. A subharmonic signal at $f_0/2$ emerges accordingly in the power spectrum, but it is over 9 dB weaker than the fundamental at f_0 and can be easily filtered out by microwave filters in practical systems.

Obviously, the feedback strength cannot be increased indefinitely. For instance, in Fig. 4(d), the slave laser enters into chaotic oscillation when the feedback strength increases to 0.060. The optical spectrum in Fig. 4(d-i) still contains the regenerative component at f_i, but the spectrum is much broadended into a continuum of chaos. The power spectrum is broadened significantly with only a small portion shown in Fig. 4(d-ii), which contains a repeating pattern in every $1/\tau$ as a characteristic of feedback-induced chaos [61]. It is worth mentioning that the different nonlinear dynamical regimes of the laser under both optical injection and feedback were recently studied in detail [8, 58], where chaotic oscillations must be avoided for microwave generation by limiting the maximal feedback strength.

According to the numerical results in Fig. 4, the P1 microwave linewidth reduces as the feedback strength increases as long as the laser remains in periodic oscillation. Experimentally, the feedback-induced narrowing of the P1 microwave linewidth was confirmed [45]. Analytically, the feedback-induced microwave linewidth reduction has not been thoroughly understood. In

#224479 - $15.00 USD Received 7 Oct 2014; revised 11 Jan 2015; accepted 15 Jan 2015; published 30 Jan 2015

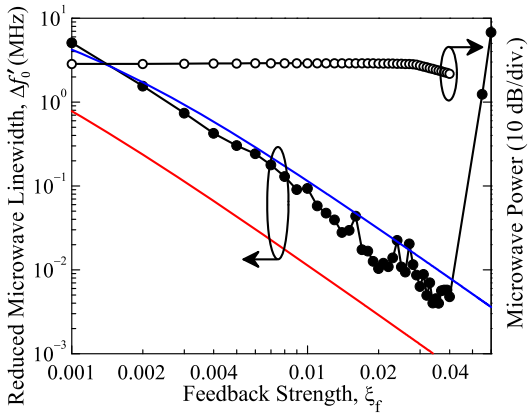

Fig. 5. Reduced microwave linewidth $\Delta f_0'$ (closed symbols) and microwave power (open symbols) as functions of the single-loop feedback strength ξ_f. The feedback delay time is fixed at τ = 2.4 ns. The estimations of $\Delta f_0'$ with $\beta = 1$ (blue) and $\sqrt{1+b^2}$ (red) are obtained from Eq. (6). The red curve is the lower-bound of $\Delta f_0'$.

order to estimate the reduced microwave linewidth $\Delta f_0'$, it is first observed from Figs. 4(a-i)–4(c-i) that the two components at f_i and $f_i - f_0$ dominate the P1 optical spectra. The regenerative component at f_i comes from a CW injection and carries nearly no linewidth. So the P1 microwave linewidth is directly translated from the optical linewidth at $f_i - f_0$. Then, by borrowing the results on feedback-induced optical linewidth narrowing in a solitary laser without injection [44,66,67], the feedback-induced optical linewidth narrowing at $f_i - f_0$ for the injected laser is estimated. As a result, the reduced microwave linewidth $\Delta f_0'$ for the P1 oscillation with feedback (ξ_f, τ) is approximated as

$$\Delta f_0' \approx \frac{\Delta f_0}{(1+\beta\gamma_c\tau\xi_f)^2}, \tag{6}$$

where Δf_0 is the microwave linewidth obtained under optical injection alone prior to applying any feedback and the feedback is assumed not to affect the optical power at $f_i - f_0$ as Figs. 4(a-i)–4(c-i) suggest. The factor β depends on the excited external cavity mode [44]. It is equal to unity for the minimum threshold mode and equal to $\sqrt{1+b^2}$ for the minimum linewidth mode. The latter case sets the lower-bound of $\Delta f_0'$. The dependencies of $\Delta f_0'$ on the feedback parameters are simulated next for verifying Eq. (6).

4.1. Reduced microwave linewidth $\Delta f_0'$ versus feedback strength ξ_f

The closed symbols in Fig. 5 show the reduced microwave linewidth $\Delta f_0'$ as the feedback strength ξ_f varies. The feedback delay time is fixed at τ = 2.4 ns. The linewidth is obtained at the P1 frequency of f_0 = 24 GHz because the injection is fixed at (ξ_i, f_i) = (0.17, 14.2 GHz). The P1 oscillation has the original microwave linewidth of Δf_0 = 22 MHz prior to application of the feedback as shown in Fig. 2(c-ii). As the feedback strength ξ_f increases, the microwave linewidth $\Delta f_0'$ decreases continuously. It reaches a minimal value of 4 kHz at ξ_f = 0.034 in Fig. 5. Further increasing the feedback strength eventually drives the laser into chaos and so broadens the linewidth.

Using Eq. (6), $\Delta f_0'$ is estimated as the blue and red curves for β = 1 and $\sqrt{1+b^2}$, respectively. Provided that the laser remains in periodic oscillation, the simulation results are above the analytical lower-bound as indicated by the red curve. The simulation results are also in

#224479 - $15.00 USD Received 7 Oct 2014; revised 11 Jan 2015; accepted 15 Jan 2015; published 30 Jan 2015

close agreement with the analytical results in blue. According to Eq. (6), when the feedback is sufficiently strong with $\xi_f \tau \gg \gamma_c^{-1}$, the reduced microwave linewidth $\Delta f_0'$ is proportional to ξ_f^{-2}.

The microwave power of the signal at f_0 is plotted as open symbols in Fig. 5. The power varies by less than 3 dB when $\xi_f < 0.04$ as long as the laser remains in periodic oscillation. Therefore, unlike conventional oscillators such as the OEOs, the feedback in Fig. 1 is not responsible for generating the P1 oscillation. The feedback merely stabilizes the fluctuations of the P1 oscillation [57].

4.2. *Reduced microwave linewidth $\Delta f_0'$ versus feedback delay time τ*

Figure 6 shows a continual reduction of $\Delta f_0'$ as the feedback delay time τ increases. The feedback strength is kept constant at $\xi_f = 0.010$. The simulation results are in closed symbols. The analytical estimations of Eq. (6) are again plotted in blue and red with $\beta = 1$ and $\sqrt{1+b^2}$, respectively. The simulated results are clearly bounded from below by the red curve. They are also in good agreement with the analytical results in blue. When the delay is sufficiently long with $\xi_f \tau \gg \gamma_c^{-1}$, the reduced linewidth $\Delta f_0'$ is proportional to τ^{-2}. The inverse-squared dependence of the linewidth on the feedback time is commonly observed, for example, in OEOs as well as in lasers at the Schawlow-Townes limit [39]. Experiments on frequency stabilization of the P1 oscillation were demonstrated with fiber loops [45], which can conveniently realize long delays with $\xi_f \tau \gg \gamma_c^{-1}$.

For completeness, it is worth mentioning that a short delay with $\xi_f \tau \sim \gamma_c^{-1}$ gives only a few external cavity modes [44]. The modes are far-separated by $1/\tau$ in causing severe frequency-shifts of the central microwave peak, which lead to drastic fluctuations of the microwave linewidth exceeding its original value without feedback [58]. Thus, for yielding phase noise reduction, short delays should be avoided. A long delay should instead be adopted according to Fig. 6.

4.3. *Phase variance versus feedback parameters (ξ_f, τ)*

The P1 oscillation phase noise improvement is illustrated through measuring the reduction of the microwave linewidth in Figs. 5 and 6. However, according to Figs. 4(a-ii)–4(c-ii), the central peak in the power spectrum is accompanied by some noisy side peaks separated by $1/\tau$. Both the non-zero linewidth and the side peaks contribute to the P1 oscillation phase noise, which can be quantified by its variance in Fig. 7. The phase noise variance is estimated by integrating the averaged single sideband of the power spectrum centered at f_0, with normalization to the microwave power, over an offset from $f_L = 3$ MHz to $f_H = 1$ GHz [22,46,52,56,58]. The phase variance is proportional to the integrated mean square timing jitter of the P1 oscillation [68]. Figure 7 is a contour map of the phase variance in the feedback parameter space (ξ_f, τ). The minimum phase variance of 0.001 rad^2 is attained at an optimal point (ξ_f, τ) = (0.034, 2.4 ns), which corresponds to Fig. 4(c-ii) with a linewidth of $\Delta f_0' = 4$ kHz. On one hand, for a fixed τ, the phase variance and the linewidth have similar dependencies on ξ_f. When ξ_f increases from zero in Fig. 7, the phase variance first experiences a progressive reduction due to central linewidth reduction and side peak suppression, but then it quickly rises up as the feedback becomes sufficiently strong to drive the laser into chaos. For example, at $\tau = 2.4$ ns, the phase variance reduces progressively as ξ_f increases up to 0.034 and then raises abruptly as the laser becomes chaotic. The linewidth in Fig. 5 follows a similar dependency on ξ_f. On the other hand, for a fixed ξ_f, the phase variance and the linewidth do not have the same dependency on τ. As τ increases, the linewidth decreases monotonically in Fig. 6, while the phase variance does not. For example, at $\xi_f = 0.034$, the contour map in Fig. 7 first shows a reduction of the phase variance until $\tau = 2.4$ ns, corresponding to the spectrum in Fig. 4(c-ii). However, as τ further

#224479 - $15.00 USD Received 7 Oct 2014; revised 11 Jan 2015; accepted 15 Jan 2015; published 30 Jan 2015

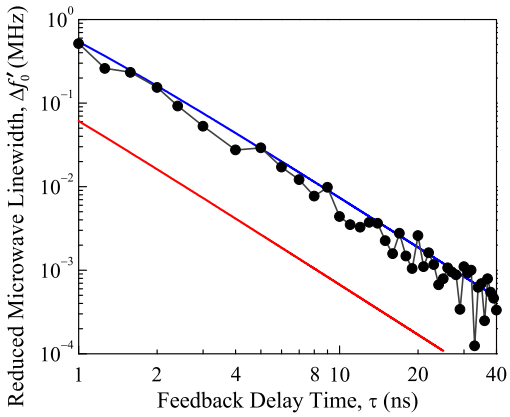

Fig. 6. Reduced microwave linewidth $\Delta f_0'$ as a function of the single-loop feedback delay time τ. The feedback strength is fixed at ξ_f = 0.010. The estimations of $\Delta f_0'$ with β = 1 (blue) and $\sqrt{1+b^2}$ (red) are obtained from Eq. (6). The red curve is the lower-bound of $\Delta f_0'$.

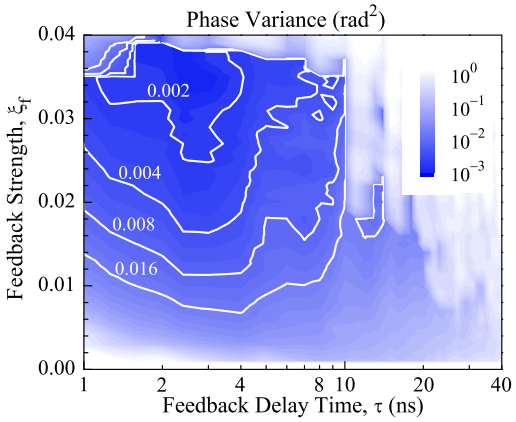

Fig. 7. Phase variance as a contour map of the single-loop feedback parameters (ξ_f, τ).

increases, the side peaks continue to move towards the central peak and increase in magnitude. This causes substantial degradation of the phase variance for large τ in Fig. 7. Comparing Figs. 6 and 7, it is clear that a continual increase of τ progressively reduces the linewidth, but this eventually causes increment of the phase variance. The side peaks need to be suppressed by modifying the feedback in the next section.

To summarize, this section illustrates the phase noise improvement of the P1 oscillation through adopting the single-loop optical feedback. The reduced microwave linewidth $\Delta f_0'$ is observed to roughly follow Eq. (6). The linewidth $\Delta f_0'$ is asymptotically proportional to ξ_f^{-2} when the feedback strengthens until the laser becomes chaotic. The linewidth is also asymptotically proportional to τ^{-2} when the feedback delay lengthens, although the side peaks grow in degrading the phase noise variance at long delays.

#224479 - $15.00 USD Received 7 Oct 2014; revised 11 Jan 2015; accepted 15 Jan 2015; published 30 Jan 2015

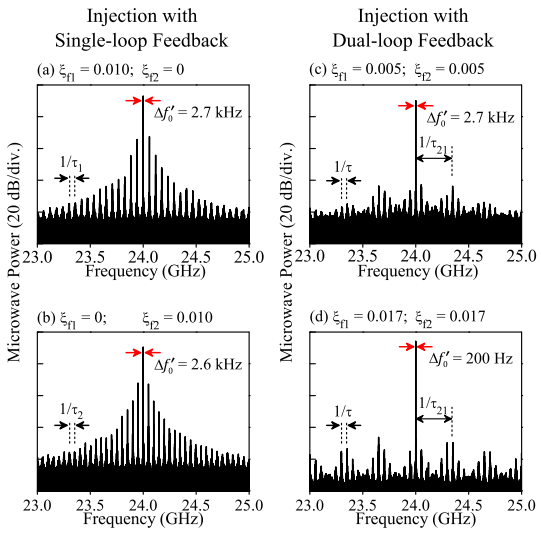

Fig. 8. Power spectra of the slave laser emission subject to optical injection with single-loop feedback (left column) or dual-loop feedback (right column). The feedback strengths (ξ_{f1}, ξ_{f2}) = (a) (0.010, 0), (b) (0, 0.010), (c) (0.005, 0.005), and (d) (0.017, 0.017). The feedback loops have delays (τ_1, τ_2) = (17 ns, 20 ns). The injection parameters are fixed at (ξ_i, f_i) = (0.17, 14.2 GHz). The reduced microwave linewidth $\Delta f_0'$ is labeled for each central peak at f_0.

5. P1 with dual-loop feedback

The previous section illustrates the inverse-square dependence of the P1 linewidth on the feedback time. A long delay time is preferred for linewidth narrowing, but the noisy side peaks grow in magnitude as the delay time increases. For the single-loop feedback, the minimum phase variance of 0.001 rad^2 is obtained at (ξ_f, τ) = (0.034, 2.4 ns) in Fig. 7, corresponding to the spectrum in Fig. 4(c-ii) with a P1 microwave linewidth of $\Delta f_0' = 4$ kHz. To further reduce the linewidth while keeping the small phase variance, the dual-loop feedback is considered in this section. The two loops have slightly different delay times so that their side peaks are misaligned in enabling the Vernier effect. The feedback parameters (ξ_{f1}, τ_1) and (ξ_{f2}, τ_2) specify the dual-loop feedback in Fig. 1. The total feedback strength is $\xi_f = \xi_{f1} + \xi_{f2}$. The average delay time is denoted as $\tau = (\tau_1 + \tau_2)/2$. The feedback delay time difference is notated $\tau_{21} = \tau_2 - \tau_1$. Figure 8 shows the results when the feedback delay times are increased to τ_1 = 17 ns and τ_2 = 20 ns, which are much longer than the original short delay of 2.4 ns in Fig. 4. Beginning with Fig. 8(a), only the loop of τ_1 is switched on with ξ_{f1} = 0.010 and ξ_{f2} = 0. The feedback with the long delay leads to the reduced central linewidth of $\Delta f_0'$ = 2.7 kHz. Similarly, in Fig. 8(b), only the loop of τ_2 is switched on with ξ_{f2} = 0.010 and ξ_{f1} = 0. The long feedback delay time again gives a small $\Delta f_0'$ of 2.6 kHz. The long delay times in Figs. 8(a)–8(b) yield the linewidths being much smaller than the linewidth of 93 kHz in Fig. 4(a-ii) for the original short delay time. However, the long delay times in Figs. 8(a)–8(b) also lead to closely packed side peaks separated by $1/\tau_1$ and $1/\tau_2$, respectively. The side peaks are close to the central peak and so are much stronger than those in Fig. 4(a-ii) for the original delay. In other words, for feedbacks with only one loop, a long delay time is preferred for central linewidth narrowing, but it is associated with strong noisy side peaks that degrade the phase variance.

Because (τ_1, τ_2) are basically incommensurate, the side peaks in Figs. 8(a)–8(b) are not perfectly aligned. When both loops are switched on in Fig. 8(c), the misalignment results in a

#224479 - $15.00 USD Received 7 Oct 2014; revised 11 Jan 2015; accepted 15 Jan 2015; published 30 Jan 2015

clear suppression of the side peaks as a Vernier effect [24, 69], which brings down the phase variance significantly. The dual-loop feedback is simulated with two equally strong feedback strengths of $\xi_{f1} = \xi_{f2} = 0.005$ such that the total feedback strength ξ_f is still 0.010. As a result, the central linewidth is maintained at $\Delta f_0' = 2.7$ kHz, but the phase variance is brought back down to the order of 0.001 rad^2. By increasing both feedback strengths to $\xi_{f1} = \xi_{f2} = 0.017$, Fig. 8(d) shows a further reduction of the central peak linewidth down to just $\Delta f_0' = 200$ Hz according to a Lorentzian fit, where the phase noise variance is less than 0.001 rad^2. Hence, the dual-loop feedback is preferred over single-loop feedback because it maintains a low phase variance while the central linewidth narrows.

The spectra with dual-loop feedback in Fig. 8(c)–8(d) contains residual side peaks separated at multiples of the reciprocal of the average delay τ. The magnitudes of the side peaks also follow an undulating envelope at the dual-loop beat frequency $1/\tau_{21} = 0.33$ GHz. Nonetheless, these side peaks are much weaker than the central peak because $1/\tau_{21}$ is much greater than the original P1 microwave linewidth of $\Delta f_0 = 22$ MHz without feedback, as in Fig. 2(c-ii). The linewidth reduction and side peaks suppression in Fig. 8 are qualitatively consistent with the reported experimental results [45].

5.1. Phase variance versus total feedback strength ξ_f

To systematically quantify the suppression of side peaks, Fig. 9 shows the phase noise variance as the total feedback strength ξ_f varies. The feedback delay times are kept constant at $\tau_1 = 17$ ns and $\tau_2 = 20$ ns. Generally, the phase variance comprises of the contribution from the Lorentzian tail of the central peak and the contribution from the side peaks. When the side peaks are completely eliminated, the ideal phase variance can be calculated by integrating the Lorentzian tail of the central peak with linewidth $\Delta f_0'$. Such an ideal phase variance is given by $\Delta f_0'(f_L^{-1} - f_H^{-1})/2\pi$ when $\Delta f_0' \ll f_L$ [22, 68]. Here, $\Delta f_0'$ is estimated by substituting the total feedback strength ξ_f and the averaged delay time τ into Eq. (6) with $\beta = 1$. The resultant estimation of the ideal phase variance is shown in Fig. 9 as the blue curve, which is always below the actual phase variance due to incomplete elimination of side peaks.

For single-loop feedback, only one loop is switched on at a time. The up-triangles are from switching on only the loop of τ_1 at strength $\xi_{f1} = \xi_f$ so that ξ_{f2} is zero. Likewise, the down-triangles are from switching on only the loop of τ_2 at strength $\xi_{f2} = \xi_f$ so that ξ_{f1} is zero. Regardless of which loop is switched on, the phase variance is always much greater than its ideal value in Fig. 9, which is due to the strong side peaks obtained at the long feedback delay times. The triangles also show the gradual reduction of phase variances as ξ_f increases, although the reduction slope is less than that of the ideal phase variance. The phase variance eventually rises at $\xi_f = 0.024$ or 0.014 for the two independent loops as the laser exhibits complex dynamics.

By contrast, the dual-loop feedback yields the phase variance as the circles indicate in Fig. 9. Both loops are switched on with equal strengths such that $\xi_{f1} = \xi_{f2} = \xi_f/2$. The phase variance from dual-loop feedback is always much smaller than that from single-loop feedback because of the suppression of the side peaks. It also reduces more quickly as the feedback strength ξ_f increases. The laser remains in P1 oscillation over a larger range of ξ_f for the dual-loop feedback as compared with the single-loop feedbacks. Until the complex dynamics emerges at ξ_f of over 0.04, the dual-loop feedback is useful for reducing the phase variance down to less than 0.001 rad^2. Therefore, although it does not completely eliminate all side peaks, the dual-loop feedback always gives a lower phase variance compared to that from the single-loop feedbacks and widens the range of the total feedback strength for P1 oscillation.

#224479 - $15.00 USD Received 7 Oct 2014; revised 11 Jan 2015; accepted 15 Jan 2015; published 30 Jan 2015

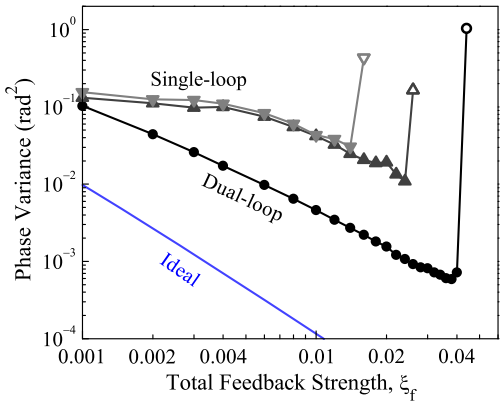

Fig. 9. Phase variance as a function of the total feedback strength ξ_f. The up- and down-triangles are from single-loop feedback at $(\xi_{f1}, \xi_{f2}) = (\xi_f, 0)$ and $(0, \xi_f)$, respectively. The circles are from dual-loop feedback at $(\xi_{f1}, \xi_{f2}) = (\xi_f/2, \xi_f/2)$. The feedback loops have delay times (τ_1, τ_2) = (17 ns, 20 ns). The ideal phase variance in blue is deduced from Eq. (6) when the side peaks are ignored.

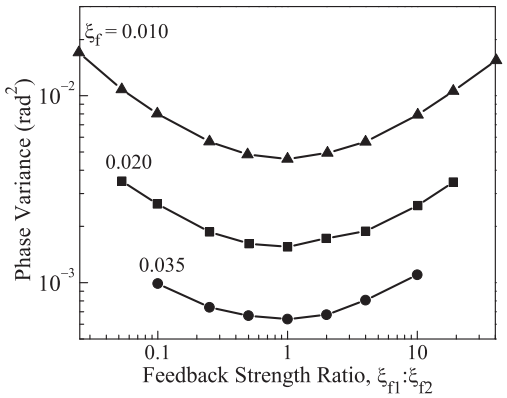

Fig. 10. Phase variance as a function of the feedback strength ratio ξ_{f1}:ξ_{f2}. The total feedback strength ξ_f is fixed at 0.010, 0.020, and 0.035 as labeled. The feedback loops have delay times (τ_1, τ_2) = (17 ns, 20 ns).

5.2. *Phase variance versus feedback strengths* (ξ_{f1}, ξ_{f2})

The effect of varying the power distribution between the two loops is considered in Fig. 10, where the phase variance is plotted against the ratio of the feedback strengths ξ_{f1} and ξ_{f2}. Regardless of the distribution of optical power feeding back through the two loops in Fig. 1, the maximal total feedback strength ξ_f is limited due to the finite optical coupling efficiency from the slave laser. So Fig. 10 keeps the total feedback strength $\xi_f = \xi_{f1} + \xi_{f2}$ constant at 0.010, 0.020, and 0.035 for the triangles, squares, and circles, respectively. The feedback delay times of the two loops remain fixed at τ_1 = 17 ns and τ_2 = 20 ns. For any ξ_f, Fig. 10 clearly shows minimization of the phase variance when the ratio ξ_{f1}:ξ_{f2} is optimized to unity. Such a feedback with equal strengths from the two loops corresponds to a filter of maximal extinction ratio, which results in effective suppression of the side peaks. In addition, as the ratio ξ_{f1}:ξ_{f2} deviates

#224479 - $15.00 USD Received 7 Oct 2014; revised 11 Jan 2015; accepted 15 Jan 2015; published 30 Jan 2015

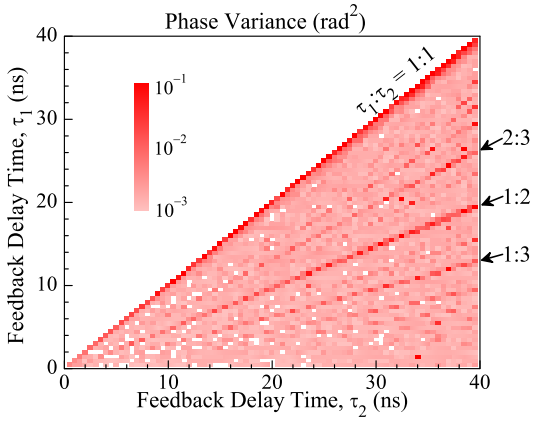

Fig. 11. Phase variance as a map of the dual-loop feedback delay times (τ_1, τ_2). The feedback strengths are kept at $\xi_{f1} = \xi_{f2} = 0.010$.

from unity at a fixed ξ_f, the dual-loop feedback becomes progressively similar to a single-loop feedback such that the side peaks become less suppressed, where the laser eventually enters other dynamical states. For instance, at ξ_f = 0.035, the laser remains in P1 oscillation only when ξ_{f1}:ξ_{f2} is between 0.1 and 10. Therefore, it is optimal to distribute the feedback power equally among the two loops for P1 oscillation phase variance minimization.

5.3. *Phase variance versus feedback delay times* (τ_1, τ_2)

The effect of varying the feedback delay times of the two loops is considered in Fig. 11. The phase variance is shown as a map of (τ_1, τ_2). The two loops are set at equal feedback strengths of $\xi_{f1} = \xi_{f2} = 0.010$. The region with $\tau_1 > \tau_2$ is not presented since the roles of the two delays are interchangeable. Over most part of the map with delays reaching 40 ns in Fig. 11, the dual-loop feedback successfully suppresses the phase variance to the order of 0.001 rad^2, which is the minimum value attainable by single-loop feedback at a much shorter delay of 2.4 ns in Fig. 7. There are also many white regions scattered in Fig. 11, which represent phase variances of even less than 0.001 rad^2. However, straight lines of relatively large phase variances emerge when τ_1 and τ_2 become commensurate. Lines with τ_1:τ_2 = 1:1, 1:2, 2:3, and 3:1 are clearly identified in Fig. 11. These rational values of τ_1:τ_2 result in strong noisy side peaks at the common multiples of the reciprocals of the delays. Moreover, at any fixed value of τ_1:τ_2, the phase variance generally increases as the delay times increase. This is due to the enhancement of the residual side peaks as their separation $1/\tau$ reduces. As the dual-loop is reduced to a single-loop when τ_1:τ_2 = 1:1, a comparison of the line along τ_1:τ_2 = 1:1 with the rest of the map confirms the superiority of dual-loop feedback over the single-loop feedback as long as commensurate (τ_1, τ_2) are avoided.

Summarizing this section, the dual-loop feedback clearly suppresses the side peaks through the Vernier effect. It allows using long delay times to reduce the P1 linewidth while maintaining a low phase variance. The two loops are preferably of equal strengths with incommensurate delays.

6. Discussion

Up to this point, the results focus on the linewidth narrowing for the P1 oscillation at f_0 = 24 GHz by optical injection of (ξ_i, f_i) = (0.17, 14.2 GHz). From a free-running optical linewidth

#224479 - $15.00 USD Received 7 Oct 2014; revised 11 Jan 2015; accepted 15 Jan 2015; published 30 Jan 2015

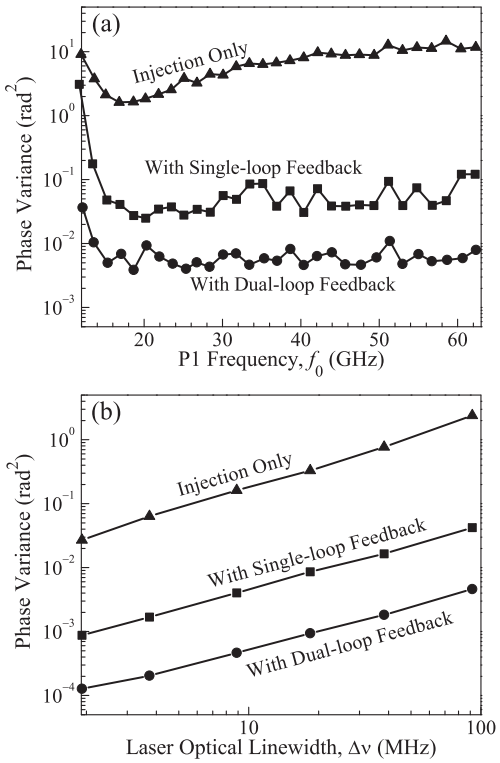

Fig. 12. Phase variance as a function of (a) P1 oscillation frequency f_0 and (b) free-running slave laser linewidth $\Delta\nu$. The laser is subject to optical injection with no feedback (triangles), single-loop feedback (squares), and dual-loop feedback (circles).

of $\Delta\nu$ = 100 MHz, the P1 oscillation of microwave linewidth Δf_0 = 22 MHz is shown in Fig. 2(c). The single-loop feedback then reduces the microwave linewidth to $\Delta f_0'$ = 4 kHz at (ξ_f, τ) =(0.034, 2.4 ns) in Fig. 4(c-ii). The dual-loop feedback further reduces the linewidth to merely $\Delta f_0'$ = 200 Hz at (τ_1, τ_2) = (17 ns, 20 ns) in Fig. 8(d), while the phase variance is maintained below 0.001 rad^2.

For completeness, the effects of the single- and dual-loop feedbacks are also investigated as the P1 oscillation frequency f_0 and the free-running laser linewidth $\Delta\nu$ are varied in Fig. 12. The phase variance is obtained without feedback, with single-loop feedback, and with dual-loop feedback for the triangles, squares, and circles, respectively. The total feedback strength is kept constant at ξ_f = 0.010. The single-loop delay time is τ = 17 ns. The dual-loop delay times are (τ_1, τ_2) = (17 ns, 20 ns) with equally distributed feedback strengths.

In Fig. 12(a), the phase variance is shown as the P1 oscillation frequency f_0 varies, where the injection parameters are chosen along the dashed line of maximal microwave power in Fig. 3. A wide tuning range of f_0 from around the relaxation resonance frequency of f_r = 10.25 GHz to over 60 GHz is shown. Increasing f_0 is associated with a slight reduction of the microwave power within about 4 dB [12, 46]. The phase variance is found to improve by one to two orders of magnitude using the single-loop feedback. Another order of magnitude of improvement is then obtained by the suppression of side peaks through the dual-loop feedback. Although the use of the sideband power ratio for the phase variance estimation becomes less accurate for the large linewidths without feedback, phase noise reduction by single- and dual-loop feedback independent of the P1 frequency is qualitatively consistent with recent experiments [45]. Also,

#224479 - $15.00 USD Received 7 Oct 2014; revised 11 Jan 2015; accepted 15 Jan 2015; published 30 Jan 2015

regardless of whether any feedback is applied, Fig. 12(a) shows a sharp increase of the phase variance as f_0 reduces in approaching f_r. This is due to the proximity to the emergence of chaotic or other nonlinear dynamics. In Fig. 12(b), the impact of the free-running linewidth $\Delta\nu$ of the slave laser is illustrated. Without any feedback, the P1 phase variance is found as directly proportional to $\Delta\nu$, where the phase variance reduction by the single- and dual-loop feedbacks are independent of $\Delta\nu$. Hence, the phase noise improvement by optical feedback is generally applicable over wide ranges of P1 frequency as well as laser linewidth.

7. Conclusion

In conclusion, the nonlinear dynamical P1 oscillation of a semiconductor laser subject to both optical injection and feedback is systematically investigated by simulation with the Langevin noise. With optical injection alone, the P1 oscillation frequency f_0 is widely tunable beyond the relaxation resonance frequency f_r, where the microwave linewidth Δf_0 varies with the injection parameters. By the P1 nonlinear dynamics, the microwave linewidth Δf_0 can even be smaller than the free-running optical linewidth $\Delta\nu$. By adding a single-loop optical feedback, the reduced microwave linewidth $\Delta f_0'$ is found as asymptotically proportional to $\xi_f^{-2}\tau^{-2}$. By modifying to a dual-loop feedback, the Vernier effect of incommensurate delay times effectively suppresses the side peaks in the power spectrum, which enables P1 linewidth narrowing at long delay times while maintaining a low phase noise variance. The results support analytical and experimental investigations on the all-optical narrow-linewidth tunable photonic microwave generation by the laser nonlinear dynamics.

Acknowledgments

The authors thank Dr. Marc Sorel for valuable discussions. This work was supported in part by a grant from the Research Grant Council of Hong Kong under Project CityU 110712, a grant from the City University of Hong Kong under Project 7002726, and a grant from the Royal Society U.K. under Project IE120157.

#224479 - $15.00 USD Received 7 Oct 2014; revised 11 Jan 2015; accepted 15 Jan 2015; published 30 Jan 2015